

Article

Advanced Fuzzy 12 DTC Control of Doubly Fed Induction Generator for Optimal Power Extraction in Wind Turbine System under Random Wind Conditions

Younes Sahri ¹, Salah Tamalouzt ¹, Sofia Lalouni Belaid ¹, Seddik Bacha ², Nasim Ullah ^{3,*}, Ahmad Aziz Al Ahamdi ³ and Ali Nasser Alzaed ⁴

¹ Laboratoire de Technologie Industrielle et de l'Information (LTII), Faculté de Technologie, Université de Bejaia, Bejaia 06000, Algeria; younes.sahri@univ-bejaia.dz (Y.S.); salah.tamalouzt@univ-bejaia.dz (S.T.); sofia.lalouni@univ-bejaia.dz (S.L.B.)

² Univ. Grenoble Alpes, CNRS, Grenoble INP*, G2Elab, F-38000 Grenoble, France; seddik.bacha@g2elab.grenoble-inp.fr

³ Department of Electrical Engineering, College of Engineering, Taif University, P.O. Box 11099, Taif 21944, Saudi Arabia; aziz@tu.edu.sa

⁴ Department of Architecture Engineering, College of Engineering, Taif University, P.O. Box 11099, Taif 21944, Saudi Arabia; alzaed@tu.edu.sa

* Correspondence: nasimullah@tu.edu.sa



Citation: Sahri, Y.; Tamalouzt, S.; Lalouni Belaid, S.; Bacha, S.; Ullah, N.; Ahamdi, A.A.A.; Alzaed, A.N. Advanced Fuzzy 12 DTC Control of Doubly Fed Induction Generator for Optimal Power Extraction in Wind Turbine System under Random Wind Conditions. *Sustainability* **2021**, *13*, 11593. <https://doi.org/10.3390/su132111593>

Academic Editor: Detlef Schulz

Received: 17 August 2021

Accepted: 9 October 2021

Published: 20 October 2021

Publisher's Note: MDPI stays neutral with regard to jurisdictional claims in published maps and institutional affiliations.



Copyright: © 2021 by the authors. Licensee MDPI, Basel, Switzerland. This article is an open access article distributed under the terms and conditions of the Creative Commons Attribution (CC BY) license (<https://creativecommons.org/licenses/by/4.0/>).

Abstract: A wind turbine (WT)-based doubly fed induction generator (DFIG) is the most often used generator in the wind conversion system market due to its advantages such as the ability of operating under variable wind speed and its high performance. However, nonlinear dynamical and parameter uncertainties of the DFIG make the controller design of this kind of system a challenging work. Thus, in this study, a novel control strategy was proposed to design the desired system dynamics, to highlight the efficacy of the proposed system, and to improve the performance of the closed-loop system. The proposed controller combines the twelve-sector direct torque control (12-DTC) and the fuzzy controller with modified rules to solve the limitations and shortcomings of the usual methods for the WT-DFIG system. All operation modes, successively and continually, were considered to reflect the true operation of WT-DFIG system subject to random wind speeds. The aims of this work was to ensure an optimal operation of the wind generator, extracting maximum power in the zone II of the WT characteristic, and limiting this power in its maximum value in the case (zone III), to transmit the power generated by the DFIG to the grid-side with minimum losses in the disturbances related to DFIG. Extensive numerical simulations were performed under MATLAB/Simulink, where the proposed fuzzy twelve direct torque control (F12-DTC) was compared with conventional nonlinear controls: conventional DTC (C-DTC) and 12-DTC. The simulation results demonstrated clearly that the proposed one had the highest performance and robustness, with a significant reduction in rotor flux and electromagnetic torque ripples and better-generated power quality with low currents' THD over the conventional strategies (C-DTC and 12-DTC).

Keywords: wind energy conversion system; non-linear control; fuzzy direct torque control; twelve-sector methodology; doubly fed induction generator; MPPT and pitch angle control

1. Introduction

The massive penetration of wind generation in the energy market is supported by the problems caused by pollution and their consequences such as climate change and lung diseases. The aim of most researchers and companies is to reduce the installation and production costs of renewable energy systems. [1,2]. The doubly fed induction generator (DFIG) is widely used for wind energy conversion systems (WECS), occupying the majority of the wind energy market due to its advantages such as the ability of operating under variable wind speeds and its high performance. This induction machine is connected to

the AC grid by its stator and via reduced size static power converters in its rotor, where it is able to be driven by variable speed. It allows to offer a decoupled active and reactive power control over a large range [3]. However, the direct grid connection of the stator makes this kind of conversion system more sensible to grid disturbances. Moreover, the non-linearity of the wind speed, the non-linear dynamics, and the uncertainties of DFIG parameters make the controller design of this kind of system a challenging work.

Wind turbine control technologies are classified according to the kind of control actuator used as: yaw control, pitch control, and generator torque control; both of the last types are discussed and studied in this article [2]. Linear and nonlinear control methods have been largely investigated in the literature and industry to address the aforementioned issues. Field-oriented control (FOC), conventional direct torque, and power controls (C-DTC/DPC) [3–6] are the basics of the DFIG control. The principal of C-DTC is the direct control of torque and flux by selecting voltage vector without using PWM block modulation nor PI regulators nor a coordinate transformer [6]. This technique is characterized by simplicity, high performance, and quick response drives as advantages compared to FOC [6]. In the opposite, C-DTC suffers from some drawbacks as variable switching frequency, important flux and torque ripples, and high-current total harmonic distortion (THD). Those disadvantages limit its use for WECSs, where the high-energy quality is necessary. Therefore, many researchers have introduced different modifications and strategies to improve the C-DTC applied to different electrical machines. An important number of research works interested in improving C-DTC applied to the induction motors [7]; although, some researchers have reported improved DTC applied to induction generators (squirrel cage induction generator and DFIG) for WECSs [8]. In order to eliminate the most important DTC drawbacks related to the variable switching frequency, a strategy called Space Vector Modulation DTC (SVM-DTC) was introduced in 1992 for induction motor drive [9]. This technique has been used a second time to control WT-DFIG [10–13], and the results of this strategy showed good performance: less torque and flux ripples and a low current THD with fewer switching losses. However, the SVM-DTC requires system parameters and a precise design of the PI controller. Additionally, PWM block modulation is required. Moreover, another method named predictive control is investigated in different works. It has been introduced as an adaptive model predictive control for a yaw system of variable speed wind turbines in [14], while it has been introduced as a predictive DPC in [15] and, in [16–18], as a predictive-DTC (P-DTC) for WT-DFIG in order to mitigate the ripples issues. The P-DTC mentioned in [16,17] is based on predicting the next variations in flux and torque; the predicted variables are utilized to select the optimal vector, while rotor voltages are applied at a constant sampling time [18]. The results showed a reduction in torque and rotor flux ripples. The sliding mode control can also improve the C-DTC; this technique is used instead of the conventional switching table and hysteresis regulators [19,20]. The simulation results showed a small reduction in rotor flux ripples and currents' THD.

Besides the modifications of conventional control strategies and the combination with different techniques, some authors have used a strategy based on the multi-level converter instead of the classical ones [21,22]. This method is characterized by the delivered power maximization with the C-DTC drawback mitigation. In [21], a multi-level-DTC (ML-DTC) was applied to control the WT-DFIG system, and the results indicated good performances under random condition; however, complexity and switching losses issues appeared. Although, the strategy is based on 21 rotor voltage vectors instead of 8, 12 sectors instead of 6, and over 180 rules instead of 9 with three- and five-level hysteresis regulators instead of two and three levels. All those modifications in SVM-DTC, P-DTC, sliding-mode-DTC (SM-DTC), and ML-DTC techniques increase the complexity of the control system and lose one of the C-DTC benefits: its simplicity. Recently, researchers in [23–27] have proposed to use the same principal of C-DTC, hysteresis regulators, and switching table but reducing the size of each sector from 60° to 30° , which will increase the number of sectors from 6 to 12 and will rise the degrees of freedom for the selection of the rotor voltage vector.

Thus, the switching table will be modified with more rules; this will improve the control accuracy, while keeping the simplicity of the control system.

Nowadays, artificial intelligence (AI) such as artificial neural networks (ANN) and fuzzy logic controllers (FLC) are investigated to improve DTC applied to WT-DFIG systems. Those techniques are mathematical methods published in scientific articles over decades and are widely used for nonlinear systems. In [28], the authors introduced an ANN to improve DTC applied to DFIG. The simulation results showed improvements by reducing flux and torque ripples, but the development of an optimal ANN is random, which hinders the performance of this strategy [7]. The FLC was first introduced in mathematics by L. Zadeh. It is an excellent simple tool for non-linear functions, and it is used in different scientific fields. In [29–31], the FLC was introduced to improve direct torque control (F-DTC) applied to the wind conversion-DFIG system, where the results showed an important reduction in rotor flux and electromagnetic torque ripples with generated current's THD. However, the authors in [30,31] treated only the sub-synchronous mode under a small range of time, which is similar to the induction generator study. Moreover, the authors did not present the powers and the generated currents' evolutions, while the main point of WECS is the generator-delivered power to supply the AC grid.

In this study, a novel control strategy was proposed to design the desired system dynamics, to highlight the efficacy of the proposed system, and, then, to improve the performance of the closed-loop system. The proposed controller combines the new twelve-sector methodology direct torque control (12-DTC) and a fuzzy logic controller with modified rules. The FC's member functions (MFs, WT-DFIG system restrictions, and drawbacks were addressed by modifying the fuzzy rules using numerical tests. All the WT-DFIG system operation modes (sub-synchronous, super-synchronous, synchronous modes, and over-speed) were considered, successively and continually, to reflect the true operation of the WT-DFIG system subject to random wind speed. The objectives of the present work were to ensure an optimal operation of the wind generator, extracting maximum power in region II of the WT characteristic and limiting this power in its maximum value in the case (region III), and to transmit the power generated by the DFIG to the grid-side with minimum losses of the disturbances related to DFIG. A comparative analysis of rotor flux and electromagnetic torque ripples of the proposed F12-DTC and the conventional controls, C-DTC and 12-DTC, was carried out and is presented in the results section. The main novel contributions reported in this study are summarized as:

- A novel-control-strategy-based non-linear modified fuzzy 12-sector-DTC (F12-DTC) was applied to the rotor side of the DFIG driven by WT under random and wide ranges of the wind profile. The new F12-DTC is investigated to solve the problem of ripples under the three DFIG operation modes and the over-speed.
- The novel approach aims directly at the causes of ripples and generated current distortions, the hysteresis regulators, and the switching table, which were replaced by the fuzzy logic controller.
- The fuzzy controller was designed based on 12 sectors instead of 6 sectors, which extends the freedom degrees of the rotor voltage vector selection. The FC's member numerical tests were used to modify functions and fuzzy rules, in order to overcome the WT-DFIG system's constraints and drawbacks.
- The treatment of all operation modes of the DFIG (sub-synchronous, super-synchronous, synchronous modes, and the over-speed) operates in a successive and continuous way, where during sub, super, and synchronous operating modes, the power is optimized using the MPPT algorithm, and, during the over-speed, the power is limited at its value using the pitch angle control.
- A graphical and analytical comparison was made between the proposed F12-DTC and both C-DTC and 12-DTC in order to show the significant improvement in the proposed strategy.

The results of comparison confirmed the good performance of the proposed F12-DTC, where the rotor flux and electromagnetic ripples and the generated currents' THD were significantly reduced, especially under the super-synchronous mode and the over-speed.

2. Materials and Methods

The overall WECS consists of a wind-turbine-driven DFIG associated with AC/DC and DC/AC power converters.

2.1. Wind Turbine Model

The following relation gives the mechanical power; it is a function of wind speed, blade radius, air density, and the power coefficient [32,33]:

$$P_{\text{mec}} = \frac{1}{2} \rho \pi R^2 v^3 C_p(\lambda, \beta) \quad (1)$$

The speed ratio and the power coefficient are given by:

$$\begin{cases} C_p(\lambda, \beta) = C_1 \left[C_2 \left(\frac{1}{\lambda_i} \right) - C_3 \beta - C_4 \right] e^{\left(\frac{C_5}{\lambda_i} \right)} + C_6 \lambda_i \\ \frac{1}{\lambda_i} = \frac{1}{\lambda + 0.08 \beta} - \frac{0.035}{1 + \beta^3} \end{cases} \quad (2)$$

The turbine torque and the tip-speed ratio are given by:

$$T_t = \frac{1}{2} C_p \frac{\rho \pi R^2}{\Omega_t} v^3 \quad (3)$$

$$\lambda = \frac{\Omega_t R_t}{v} \quad (4)$$

The mechanical torque and the mechanical speed are described by the following equations:

$$T_{\text{mec}} = \frac{T_t}{G} \quad (5)$$

$$\Omega_{\text{mec}} = \Omega_t G \quad (6)$$

$$J \frac{d\Omega_{\text{mec}}}{dt} + f_v \Omega_{\text{mec}} = T_{\text{mec}} - T_{\text{em}} \quad (7)$$

2.2. The Working Zones of Wind Turbine System

Figure 1 presents the operational zones of a variable-speed wind turbine. Zone I is an area where wind speed is very low, and the WT is cut-out. Zone II: when the wind speed is greater to the cut-in speed, the MPPT algorithm is used to extract the maximum amount of power ($\beta = 0^\circ$). Pitch angle control (Zone III) is used when wind speed becomes greater than the nominal wind speed. The system limits the output power at its nominal amount by adjusting the pitch angle. Zone IV: the DFIG rotor is disengaged from the turbine when the maximum wind speed is attained, interrupting the power production [6].

2.3. Maximum Power Point Tracking Algorithm

The WT power characteristic in the second zone had a non-linear curve and a parabolic shape, which permits the pitch angle to be zero and the power coefficient to reach its maximum value [33,34]. The DFIG's speed was tied to a reference from the MPPT algorithm for maximum wind power tracking, as shown in Figure 2. The electromagnetic torque reference was expressed as follows [8,34]:

$$T_{\text{em-ref}} = \frac{\rho}{2} \frac{C_{p-\text{max}}}{\lambda_{\text{opt}}^3} \pi \frac{R_t^5}{G} \Omega_{\text{mec}}^2 \quad (8)$$

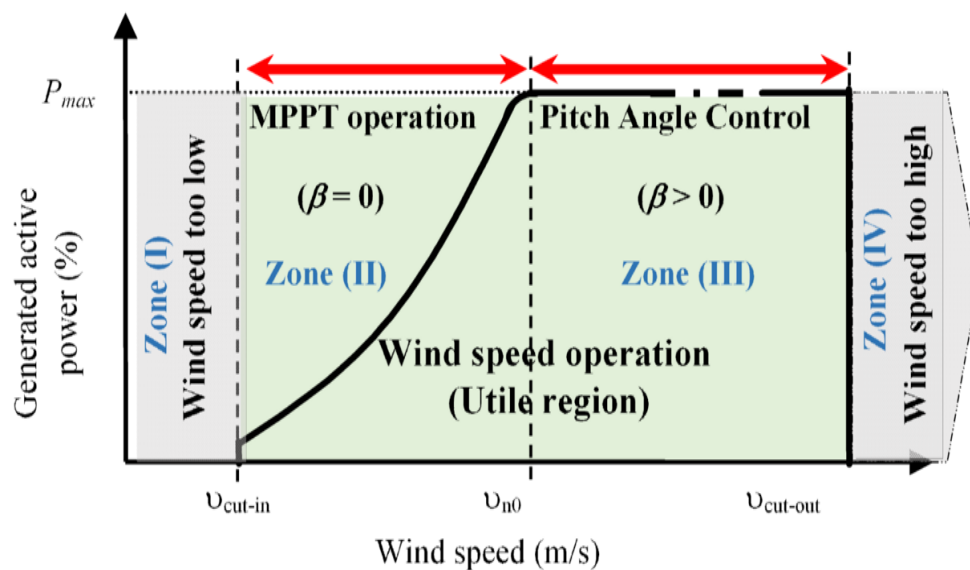


Figure 1. Wind turbine characteristic with different operating zones.

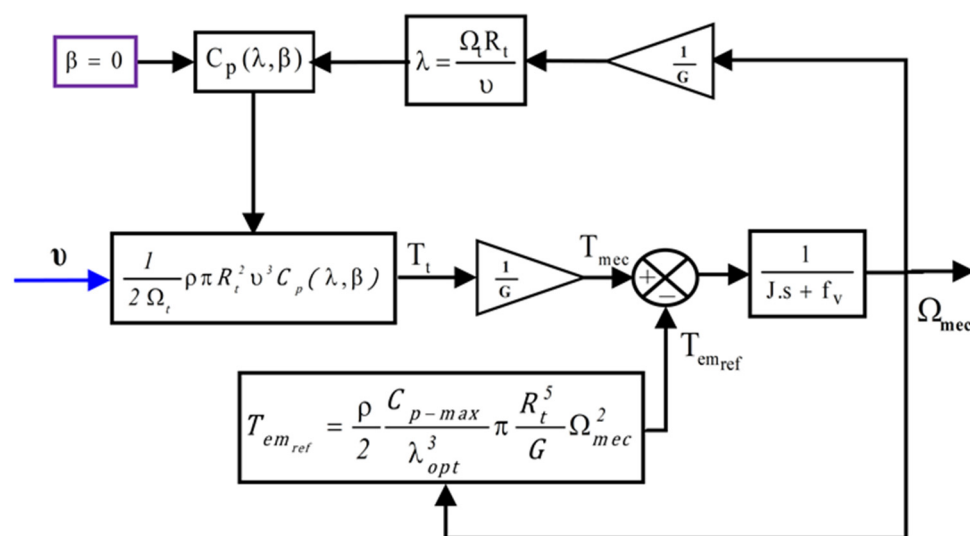


Figure 2. Bloc diagram of wind energy conversion system with MPPT algorithm.

2.4. Pitch Angle Control

To protect the electrical generator system, the blade angle control limits the delivered power to its nominal value when the wind speed exceeds the nominal value (the overspeed). However, the extraction power maximization means that the power produced is regulated; therefore, the PI regulator ensures the generation of torque reference, as presented in Figure 3 [6].

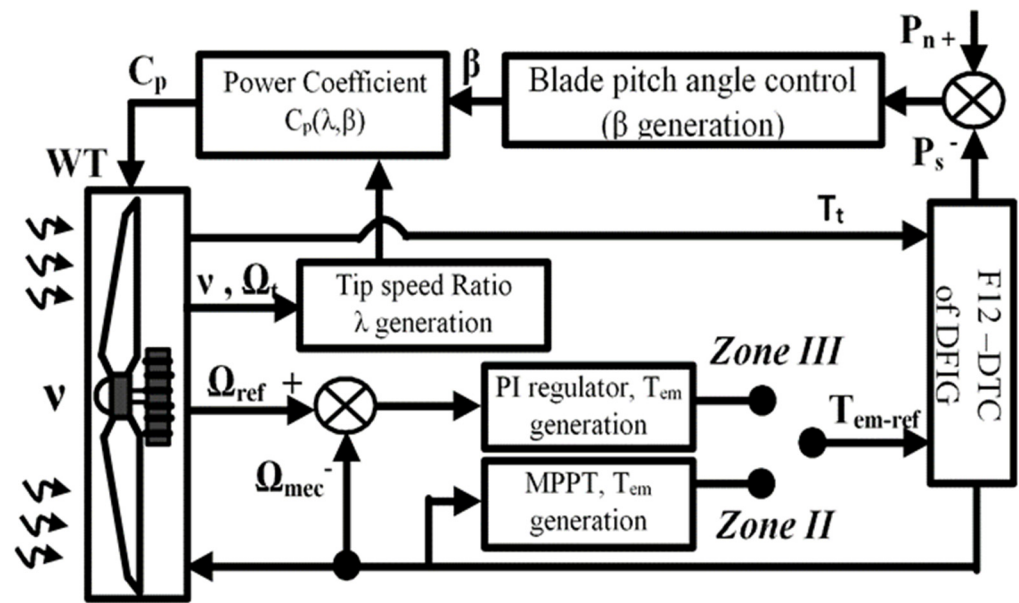


Figure 3. Description scheme of wind turbine control, MPPT, and blade angle control.

2.5. DFIG Modelling

The DFIG is modelled by voltage and magnetic equations. These equations are rewritten in d-q frames rotating at the synchronous pulsation as given in Equations (9) and (10) [20,31–33]:

$$\begin{cases} V_{sd} = R_s i_{sd} + \frac{d\varphi_{sd}}{dt} - \omega_s \varphi_{sq} \\ V_{sq} = R_s i_{sq} + \frac{d\varphi_{sq}}{dt} + \omega_s \varphi_{sd} \\ V_{rd} = R_r i_{rd} + \frac{d\varphi_{rd}}{dt} - \omega_r \varphi_{rq} \\ V_{rq} = R_r i_{rq} + \frac{d\varphi_{rq}}{dt} + \omega_r \varphi_{rd} \end{cases} \quad (9)$$

The DFIG magnetic flux equations in the d-q synchronous frame are given by:

$$\begin{cases} \varphi_{sd} = L_s i_{sd} + M i_{rd} \\ \varphi_{sq} = L_s i_{sq} + M i_{rq} \\ \varphi_{rd} = L_r i_{rd} + M i_{sd} \\ \varphi_{rq} = L_r i_{rq} + M i_{sq} \end{cases} \quad (10)$$

3. Descriptions of the Treated Control Methods and the Proposed Strategy

3.1. Conventional Direct Torque Control Description

Over decades, the C-DTC has been used to control WT-DFIG systems. It is based on direct torque and flux regulation by selecting the optimal voltage vector, without measuring speed, flux, or torque, in order to make the rotor flux rotate and obtain the required torque demand. The only measurements used are the DC voltage and the machine rotor side currents.

The rotor flux is evaluated from its components in α - β axes [31,33]:

$$\begin{cases} \varphi_{r\alpha} = \int (V_{r\alpha} - R_r i_{r\alpha}) \\ \varphi_{r\beta} = \int (V_{r\beta} - R_r i_{r\beta}) \end{cases} \quad (11)$$

$$\varphi_r = \sqrt{\varphi_{r\alpha}^2 + \varphi_{r\beta}^2} \quad (12)$$

The torque is calculated using the flux components and the rotor currents components in the rotor frame [31,33]:

$$T_{em} = P(\varphi_{r\alpha} i_{r\beta} - \varphi_{r\beta} i_{r\alpha}) \quad (13)$$

The rotor flux angle θ_r is given by:

$$\theta_r = \tan^{-1}\left(\frac{\varphi_{r\beta}}{\varphi_{r\alpha}}\right) \quad (14)$$

The rotor flux space is split into six sectors (60° each). The errors are converted into digital numbers (1, 0, or -1) by using hysteresis regulators. The switching vector of the voltage source inverter is selected using the flux sector and the outputs hysteresis bands of flux and torque. The optimal voltage vector is chosen based on the switching table, which is presented in Table 1 [30].

Table 1. Conventional DTC commutation table of wind conversion-DFIG system.

H_{φ_r}	$H_{T_{em}}$	N					
		1	2	3	4	5	6
-1	-1	V_5	V_6	V_1	V_2	V_3	V_4
	0	V_7	V_0	V_7	V_0	V_7	V_0
	+1	V_3	V_4	V_5	V_6	V_1	V_2
+1	-1	V_6	V_1	V_2	V_3	V_4	V_5
	0	V_0	V_7	V_0	V_7	V_0	V_7
	+1	V_2	V_3	V_4	V_5	V_6	V_1

3.2. Direct-Torque-Control-Based Twelve Sectors Applied to WT-DFIG System

The direct-torque-control-based twelve sectors methodology has been introduced to control doubly fed induction machines for both motor and generator operations without any driving in [23] and to control DFIG driven by WT in [24]. In these references, researchers analyzed the performances for variable mechanical speed dealing only with the sub-synchronous mode, where the super-synchronous and synchronous modes and the over-speed were not investigated to show DFIG's benefits in terms of performance improvement. Moreover, an important improvement to the 12-DTC is introduced in the present section.

The 12-DTC control based on C-DTC principal used the same equations to estimate the required parameters: the rotor flux, the electromagnetic torque, and the rotor flux sector. The electromagnetic torque and rotor flux errors were digitalized using two- and five-level hysteresis bands, respectively, as presented in Figures 4 and 5, instead of the two- and three-level hysteresis of C-DTC. In order to increase the control precision for the vector selection, the sectors number was increased from 6 to 12, of 30° each sector instead of 60° . Each sector n ($n = 1, 2, 3, \dots, 12$) is defined by the Equation (15), and the sectors and the rotor voltage vectors are presented in Figure 6.

$$\frac{\pi(n-1)}{6} \leq \theta_n < \frac{\pi.n}{6} \quad (15)$$

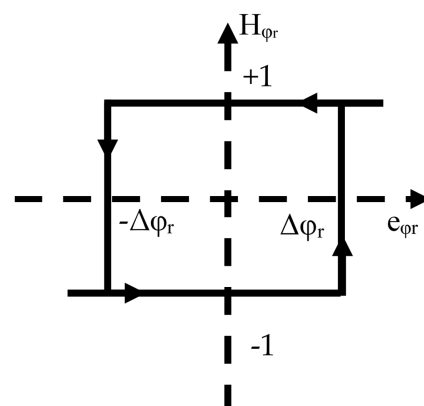


Figure 4. The rotor flux two-level hysteresis bands.

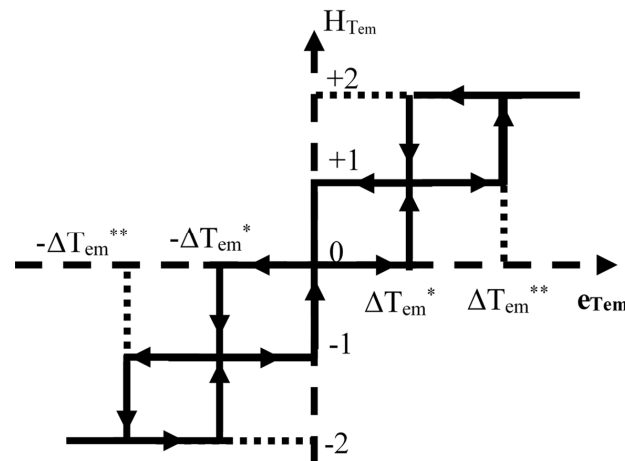


Figure 5. The electromagnetic torque five-level hysteresis bands. ΔT_{em}^* : small electromagnetic error, ΔT_{em}^{**} : large electromagnetic error.

The optimal vector selection was based on the 12-DTC switching table, which is presented in Table 2. This last uses three inputs: the digital values of errors ($H_{T_{em}}$ and H_{φ_r}) and the rotor flux sector. In order to understand the fundamental idea of the selection process, the DTC principal was investigated, where the development of the electromagnetic torque and the rotor flux equations give Equation (16) [35]:

$$T_{em} = \frac{P}{2} \frac{M}{\sigma L_s L_r} |\varphi_s| |\varphi_r| \sin \gamma \tag{16}$$

The stator flux ($|\varphi_s|$) has a constant magnitude because the DFIG is connected directly to an infinite AC grid (ideal grid) by its stator. From this fact ($|\varphi_s| = cst$) and Equation (16), the variations in electromagnetic torque were due to the variation in the rotor flux magnitude ($|\varphi_r|$) and the angle between the rotor flux and the stator flux (γ). Therefore, to obtain a fast response with accuracy, the rotor flux magnitude must be kept as constant possible, and the angle between the rotor flux and the stator flux must be controlled using the accurate vector. The fundamental idea is explained further in Figure 6.

On the other side, the null voltage vectors (V_0 and V_7) that concern $H_{T_{em}} = 0$ (when the torque must be maintained) were added compared to the switching table used in [23,24] to have more control precision.

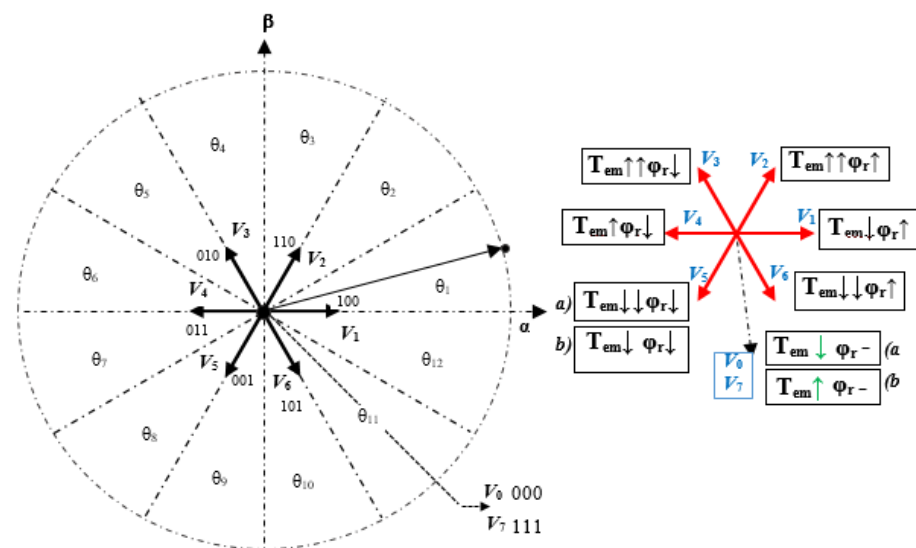


Figure 6. The influence of principal of 12-DTC, sectors, and rotor voltage vectors (a) during sub- and synchronous modes and (b) during super-synchronous mode and over-speed.

In Figure 6, the variation in torque and flux was influenced by the voltage vectors in different manners. Each arrow defines the behavior of each vector: $\uparrow\uparrow$ important increase, \uparrow normal increase, $\downarrow\downarrow$ important decrease, and \downarrow normal decrease in torque or flux $\uparrow\uparrow$, $\downarrow\downarrow$ important or normal increase/decrease depending on the time of application.

The studied system controlled by the 12-DTC is presented in Figure 7.

Table 2. Switching table of the 12-DTC for WT-DFIG system.

Sector N		θ_1	θ_2	θ_3	θ_4	θ_5	θ_6	θ_7	θ_8	θ_9	θ_{10}	θ_{11}	θ_{12}
1	$H_{\varphi r}$												
	$H_{T_{em}}$												
	2	V_2	V_3	V_3	V_4	V_4	V_5	V_5	V_6	V_6	V_1	V_1	V_2
	1	V_2	V_2	V_3	V_3	V_4	V_4	V_5	V_5	V_6	V_6	V_1	V_1
	0	V_0	V_7	V_7	V_0	V_0	V_7	V_7	V_0	V_0	V_7	V_7	V_0
-1	2	V_3	V_4	V_4	V_5	V_5	V_6	V_6	V_1	V_1	V_2	V_2	V_3
	1	V_4	V_4	V_5	V_5	V_6	V_6	V_1	V_1	V_2	V_2	V_3	V_4
	0	V_7	V_0	V_0	V_7	V_7	V_0	V_0	V_7	V_7	V_0	V_0	V_7
	-1	V_7	V_5	V_0	V_6	V_7	V_1	V_0	V_2	V_7	V_3	V_0	V_4
	-2	V_5	V_6	V_6	V_1	V_1	V_2	V_2	V_3	V_3	V_4	V_4	V_5

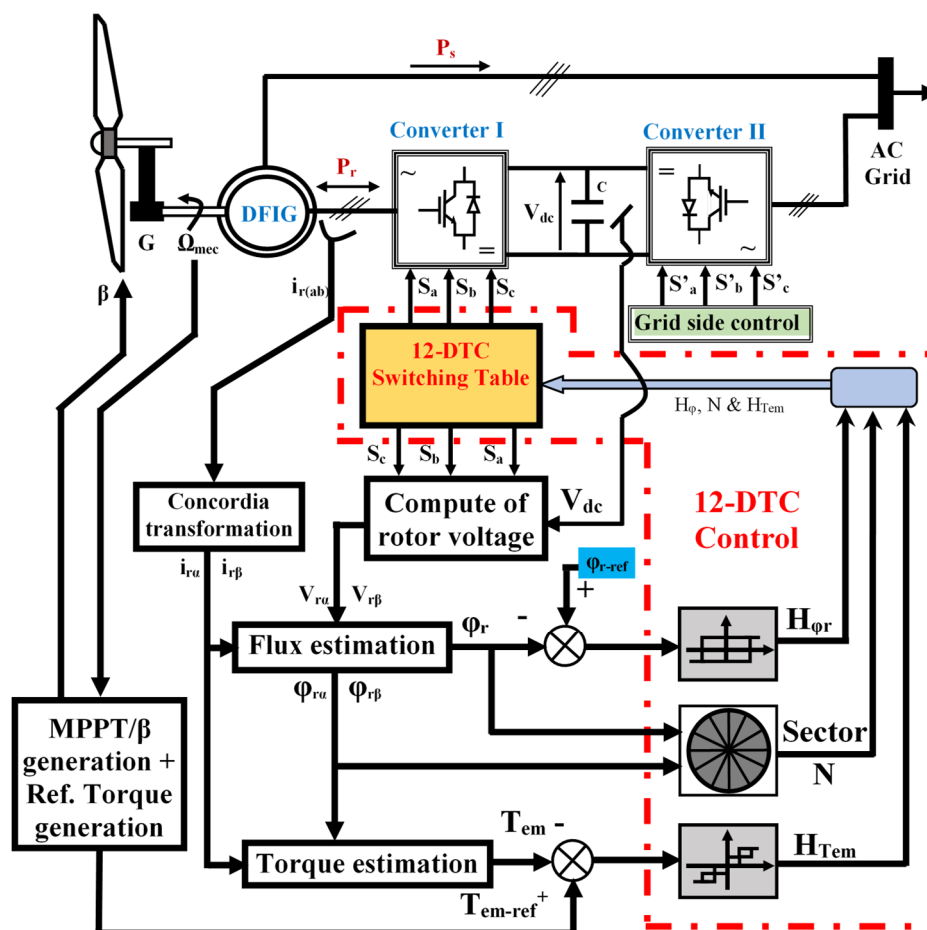


Figure 7. The 12-DTC applied to wind turbine DFIG system.

3.3. Proposed Controller Design Process of the Proposed F12-DTC

As described above, the C-DTC and 12-DTC are based on the hysteresis regulators and the switching table, which cause important rotor flux ripples and electromagnetic ripples and high generated current THD. Therefore, the proposed novel approach was aimed

directly to replace the hysteresis regulators and the switching table of the conventional controls by one fuzzy logic controller (FLC). This latter component was introduced in order to minimize all ripples and to reduce generated current harmonics, based on the FLC, which is an artificial intelligence tool that calculates quickly and instantly the optimal vector. However, the hysteresis regulator does not change the digital error until the error reaches the hysteresis band, which creates a delay in the response. Moreover, there are four tools: two different hysteresis regulators, the sector selector, and the switching table, but the proposed control used only one tool (FLC), which improves the dynamic system.

The design process of the proposed fuzzy twelve direct torque control (F12-DTC) was based on the principal of the 12-DTC control system, and it requires several steps. Firstly, the methodology of twelve sectors was used instead of six, which highly increased the selection freedom on the flux area. Secondly, the FLC was adopted based on twelve-sector methodology and direct torque control to design the desired system dynamics and to highlight the efficiency of the proposed system.

Remark 1. The FLC was designed after several numerical tests to obtain optimal fuzzy rules and optimal inputs and outputs of member functions. For the studied system, the rotor flux error, $e_{\varphi r}$, the torque error, $e_{T_{em}}$, and the rotor flux angle, θ_r , were the inputs of the fuzzy controller. The output was the selected rotor voltage vector V_j ($j: 0, \dots, 7$).

3.3.1. Fuzzification

The first step of the proposed F12-DTC process consisted in converting the system inputs into fuzzy sets, using fuzzy linguistic terms and membership functions. The fuzzification process was inspired from the behavior of both five- and two-level hysteresis regulators for the torque and flux error inputs, and it was inspired from the sector selector for the rotor flux angle input. The fuzzification convert the three inputs into variables using MFs:

- MFs of torque error ($e_{T_{em}}$) are five linguistic variables: negative large (NL), positive large (PL), negative small (NS), positive small (PS), and zero (Z). The NL and PL are formed by trapezoidal MFs, and the NS, PS, and Z are formed by triangular MFs, as shown in Figure 8.
- MFs of flux error ($e_{\varphi r}$) are three linguistic variables: negative (N), positive (P), and zero (Z). N and P are formed by trapezoidal MFs, and Z is formed by triangular MFs, as shown in Figure 9.
- MFs of the rotor flux angle are twelve linguistic variables: $\theta_1, \dots, \theta_{12}$; they are formed by triangular MFs, as illustrated in Figure 10.

The FLC output of the selected rotor voltage vector V_j are represented by sharp triangular MFs, as presented Figure 11.

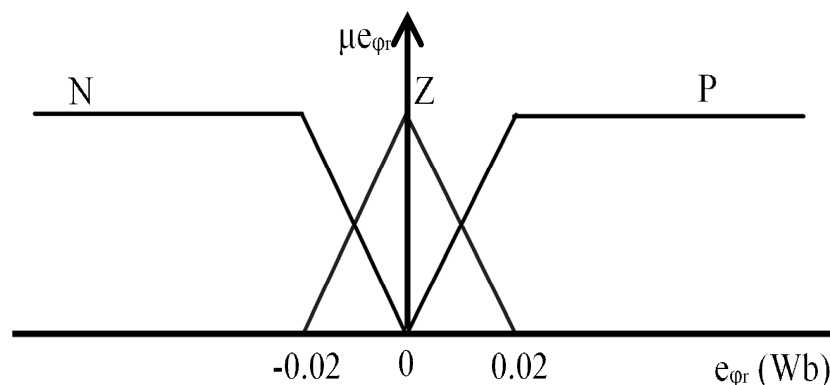


Figure 8. MF of the rotor flux error input.

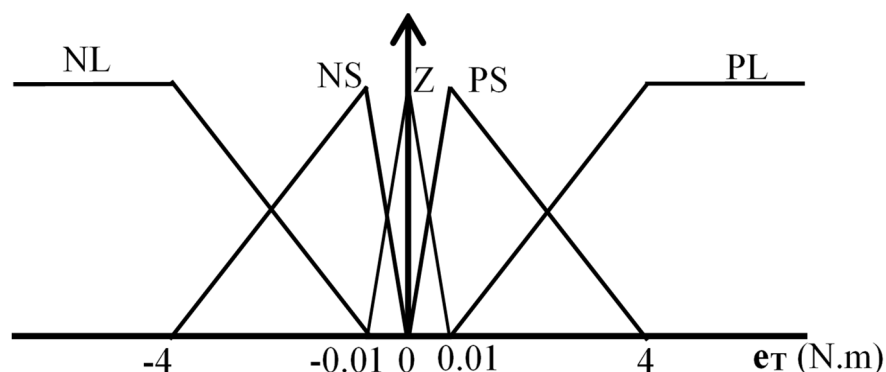


Figure 9. MF of the electromagnetic torque error input.

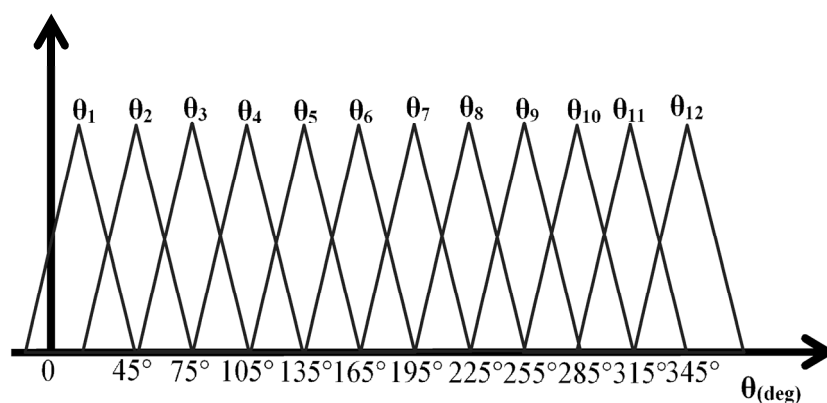


Figure 10. MF of the rotor flux angle input.

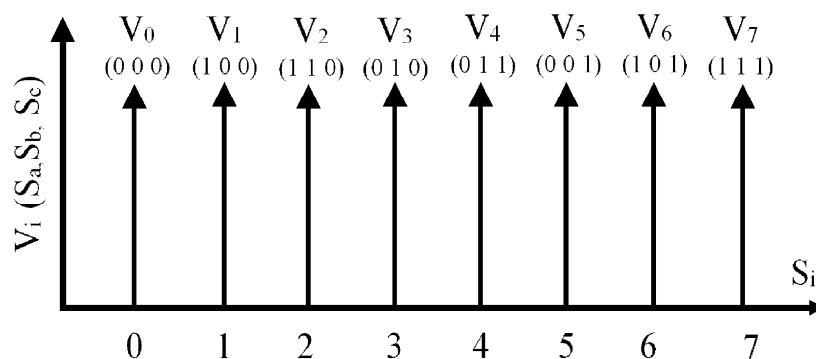


Figure 11. MF of the output, the rotor voltage vectors.

3.3.2. Fuzzy Rules

The fuzzy rules are inspired from the switching table of the DTC-based twelve sector methodology. Every condition that is used in the switching table is one rule that is based on the AND operator, in order to have a similar mission of one condition. However, there are three inputs. The first input was divided into 3 MFs (inspired from the two-level hysteresis regulator); the second input was divided into 5 MFs (inspired from the five-level hysteresis regulator); and the third input was divided into 12 MFs (inspired from the twelve sectors of the sector selector). Therefore, it must be 180 rules ($3 \times 5 \times 12$) to cover all possibilities that can be in any moment of the system operation.

After the inputs are fuzzified, an appropriate rule-base should be developed using the inputs and the outputs. An example of one rule process (the first that presented in Table 3): IF (e_{φ_r} is NL) AND ($e_{T_{em}}$ is N) AND (θ is θ_1) THEN (V_n will be V_5).

This step consists in the development of a suitable rules set; those rules will be designed using the input and output variables and MFs based on the <If condition and the

conclusion>. A Mamdani-type fuzzy inference system was used to perform the fuzzy logic switching controller, and the fuzzy rules were developed using the inputs and outputs. Those rules are presented in Table 3. There are 180 rules based on MFs for three inputs ($3 \times 5 \times 12$), using the AND operator. The fuzzy rules surfaces were performed under Matlab Fuzzy Toolbox, as illustrated in Figure 12.

Table 3. Fuzzy rules table of the proposed fuzzy twelve direct torque control.

$e_{\phi r}$	$e_{T_{em}}$	Sectors											
		θ_1	θ_2	θ_3	θ_4	θ_5	θ_6	θ_7	θ_8	θ_9	θ_{10}	θ_{11}	θ_{12}
N	NL	V ₅	V ₆	V ₆	V ₁	V ₁	V ₂	V ₂	V ₃	V ₃	V ₄	V ₄	V ₅
	NS	V ₅	V ₅	V ₆	V ₆	V ₁	V ₁	V ₂	V ₂	V ₃	V ₃	V ₄	V ₄
	Z	V ₀	V ₇	V ₇	V ₀	V ₀	V ₇	V ₇	V ₀	V ₀	V ₇	V ₇	V ₀
	PS	V ₃	V ₄	V ₄	V ₅	V ₅	V ₆	V ₆	V ₁	V ₁	V ₂	V ₂	V ₃
	PL	V ₃	V ₃	V ₄	V ₄	V ₅	V ₅	V ₆	V ₆	V ₁	V ₁	V ₂	V ₂
Z	NL	V ₅	V ₆	V ₆	V ₁	V ₁	V ₂	V ₂	V ₃	V ₃	V ₄	V ₄	V ₅
	NS	V ₀	V ₀	V ₇	V ₇	V ₀	V ₀	V ₇	V ₇	V ₀	V ₀	V ₇	V ₇
	Z	V ₀	V ₀	V ₇	V ₇	V ₀	V ₀	V ₇	V ₇	V ₀	V ₀	V ₇	V ₇
	PS	V ₃	V ₃	V ₄	V ₄	V ₅	V ₅	V ₆	V ₆	V ₁	V ₁	V ₂	V ₂
	PL	V ₂	V ₃	V ₃	V ₄	V ₄	V ₅	V ₅	V ₆	V ₆	V ₁	V ₁	V ₂
P	NL	V ₆	V ₁	V ₁	V ₂	V ₂	V ₃	V ₃	V ₄	V ₄	V ₅	V ₅	V ₆
	NS	V ₆	V ₁	V ₁	V ₂	V ₂	V ₃	V ₃	V ₄	V ₄	V ₅	V ₅	V ₆
	Z	V ₇	V ₇	V ₀	V ₀	V ₇	V ₇	V ₀	V ₀	V ₇	V ₇	V ₀	V ₀
	PS	V ₂	V ₂	V ₃	V ₃	V ₄	V ₄	V ₅	V ₅	V ₆	V ₆	V ₁	V ₁
	PL	V ₂	V ₂	V ₃	V ₃	V ₄	V ₄	V ₅	V ₅	V ₆	V ₆	V ₁	V ₁

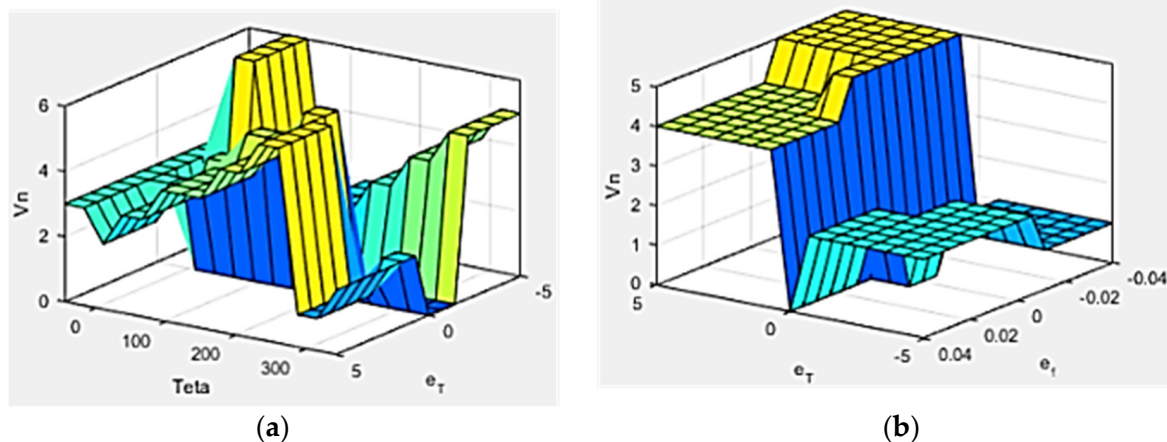


Figure 12. The obtained fuzzy rules surfaces under Matlab Fuzzy Toolbox. (a) The fuzzy surface of the flux angle and the electromagnetic torque error with the voltage vectors, (b) the fuzzy surface of the electromagnetic torque and flux errors with the voltage vectors.

3.3.3. Defuzzification

Defuzzification consists in combining rules and converting the resulting fuzzy sets into real values. The small of maximum (SoM) method was used, which calculates the MF's value. The FLC calculates the selected vector V_j ($j: 0, \dots, 7$), which will be applied to the inverter. Therefore, the V_j is converted to commutation signals for inverter (Sa, Sb, and Sc) by a Boolean expression (0 or 1).

The general structure of the proposed F12-DTC applied to WT-DFIG system connected to the AC grid is presented in Figure 13.

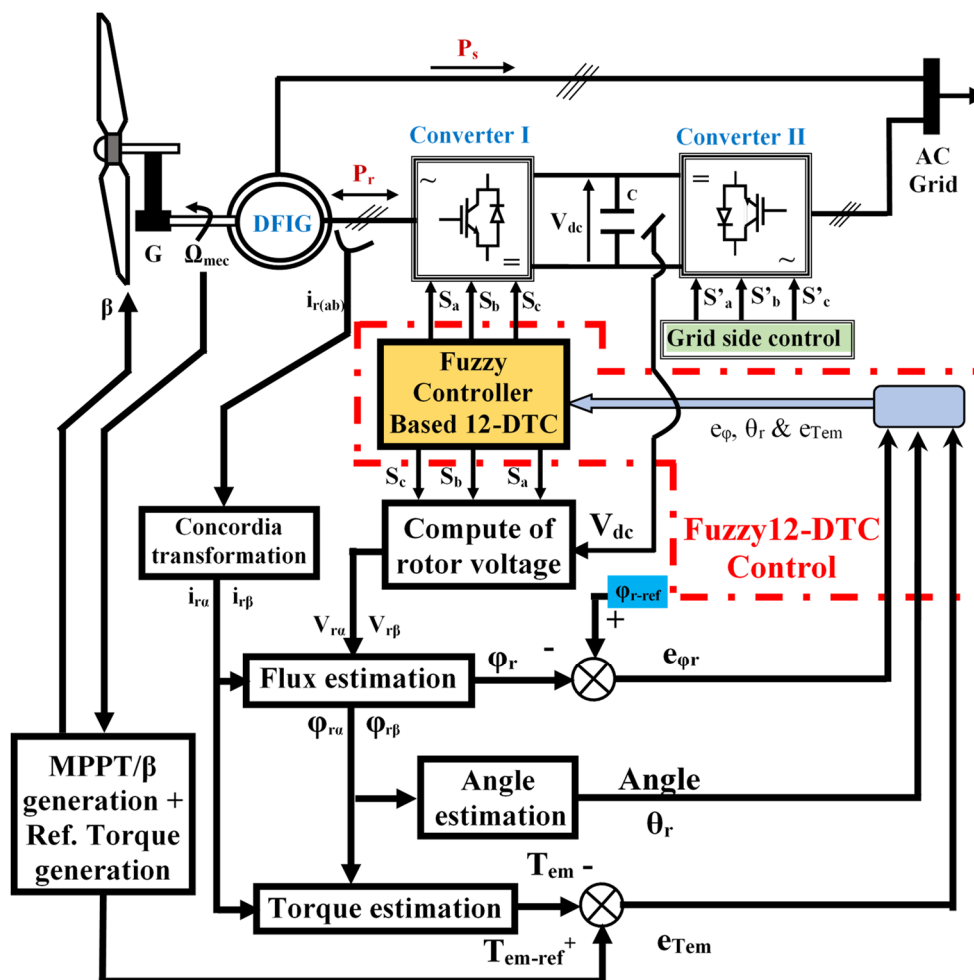


Figure 13. Description scheme of fuzzy twelve direct torque control applied to wind conversion-DFIG system.

4. Simulation Results and Discussion

Simulation tests of the proposed fuzzy twelve direct torque control (F12-DTC) applied to DFIG driven by a wind turbine were performed under MATLAB/Simulink, the simulation scheme is presented in Appendix A. This work was done using random behavior of wind speed, allowing all DFIG’s operation modes in a continuous and successive manner: sub, super, and synchronous modes with the case of over-speed. The system parameters used in simulation are presented in Table 4 [36]. This section is divided into two parts: Section 4.1. Robustness and tracking tests of references for random profile of the set-points and Section 4.2. Obtained results summary with comparison.

Table 4. Wind conversion-DFIG system parameters.

Parameter	Value	Parameter	Value
Rated Power (kW)	7.5	V_{dc} (V)	880
Frequency (Hz)	50	R_s (Ω)	1.02
Pole (pairs)	3	R_r (Ω)	0.8
R_t (m)	3.24	M (H)	0.0664
G	5.065	L_s (H)	0.093
ρ (kg/m^3)	1.1225	L_r (H)	0.081

4.1. Robustness and Tracking Tests of References for a Random Profile of The Set-Points

The performance and good quality of the proposed control were carried out in such a manner as to recreate some limitations that reflect the real behavior of the wind. The wind

speed can be modelled by a variable function, driving the DFIG in all its operation modes (synchronous, super-synchronous, sub-synchronous, and the over-speed modes). The wind speed and the DFIG mechanical speed are given in Figure 14. The MPPT technique ensures the tracking of the maximum power by generating the electromagnetic torque reference instantaneously at its maximum value in region II of the WT-characteristic, as given in Figure 1, in order to be used for tracking by the proposed control strategy (F12-DTC). However, in region III, the pitch angle control will ensure the generation of the optimal electromagnetic torque reference, where the extraction of the optimal power in this region is limited to the maximal value of the DFIG output power, which is the rated power value. A good tracking of the electromagnetic torque and rotor flux references with fewer ripples and low generated currents THD will ensure an optimal generated power with better quality, which will supply the AC grid. The MPPT set the power coefficient at its maximum value ($C_{p-max} = 0.49$) and the speed ratio λ to its optimal value ($\lambda_{opt} = 9$) during the operation modes of zone II (MPPT zone, Figure 2). By contrast, the pitch angle control varied the WT blade angle and the speed ratio during the over-speed mode, in order to limit the DFIG speed, the electromagnetic torque, and the generated power at their maximum values, as illustrated in Figures 14–16.

The electromagnetic torque (T_{em}) evolution depends on the mechanical speed, and it follows its reference very well, as presented in Figure 16. This ensure the optimal power extraction. The rotor flux also follows its reference with a constant value of 1.2 Wb with low ripples, as shown in Figure 17. In the plane (α, β), it takes a circular shape with a constant amplitude (1.2 Wb), as presented in Figure 18. In both modes: sub and super-synchronous, the flux components ($\varphi_{r\alpha}, \varphi_{r\beta}$) take a sinusoidal form, whereas, during the synchronous mode, the flux components ($\varphi_{r\alpha}, \varphi_{r\beta}$) are continuous, as illustrated in Figure 19.

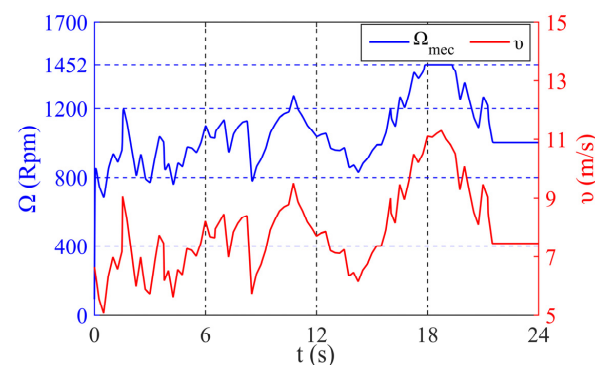


Figure 14. Wind speed and mechanical speed waveforms.

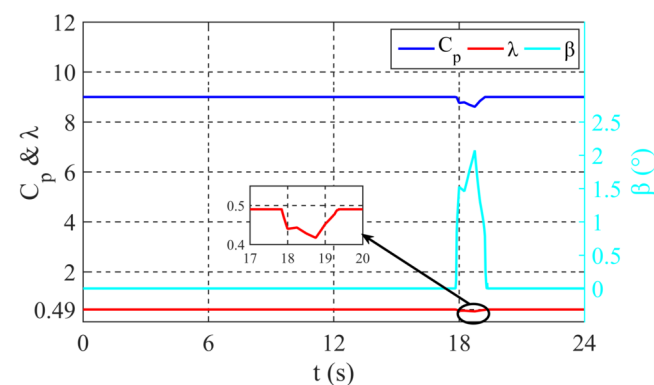


Figure 15. Power coefficient, speed ratio, and WT blade angle evolutions.

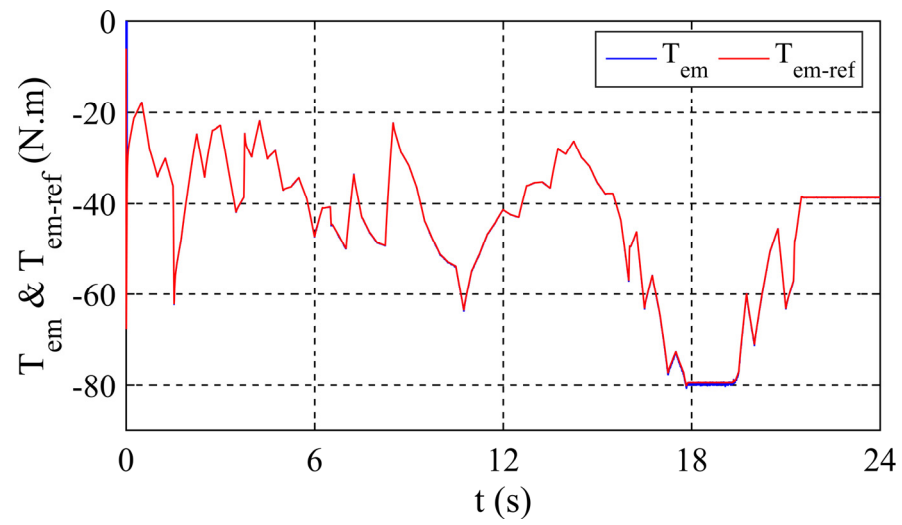


Figure 16. Electromagnetic torque and its reference.

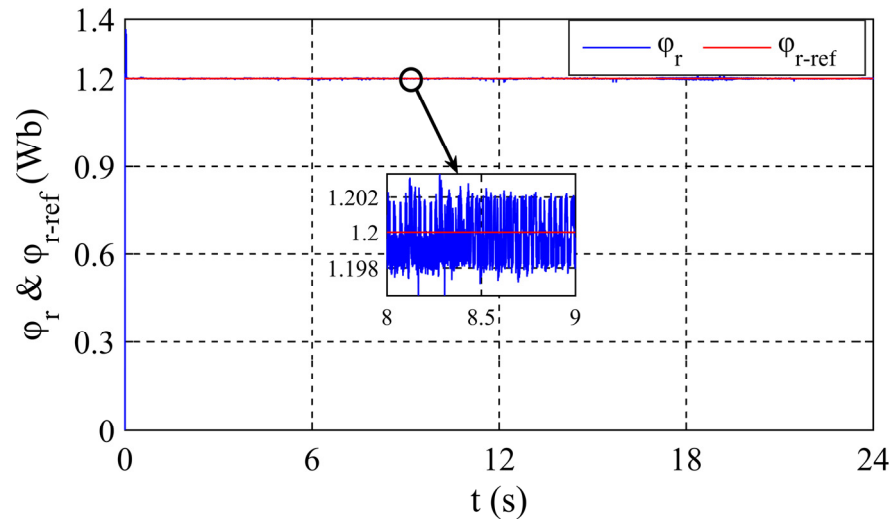


Figure 17. Rotor flux and its reference.

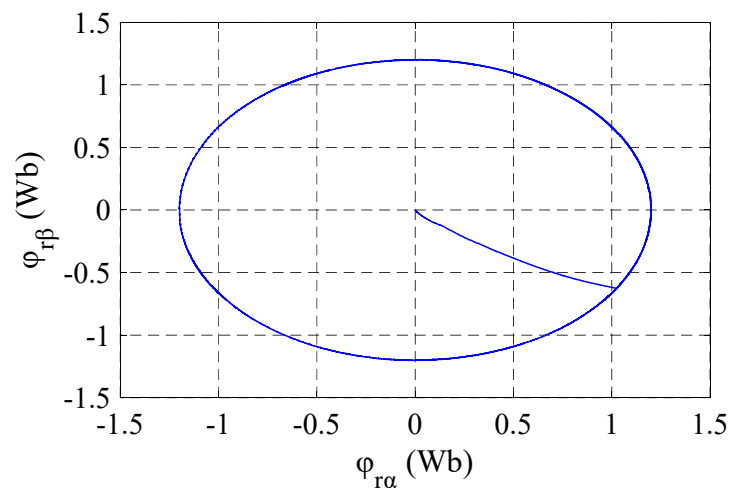


Figure 18. Waveform of the rotor flux in α - β rotor frame.

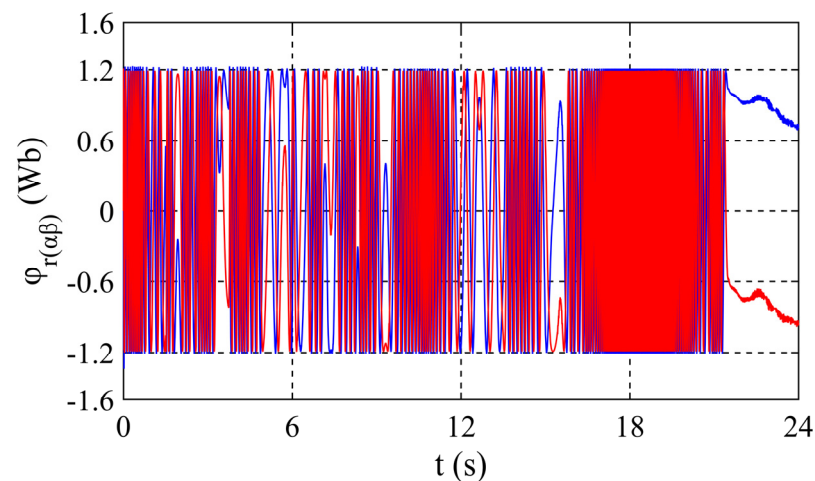


Figure 19. Evolution of rotor flux in the α - β frame ($\varphi_{r\alpha}$, $\varphi_{r\beta}$).

The evolution of the generated currents $I_{s(abc)}$ had a sinusoidal form with a constant frequency (50 Hz), as presented in Figure 20. These currents supply the AC-grid directly without any filters.

The evolution of the rotor currents $I_{r(abc)}$ had a sinusoidal form during sub and super-synchronous modes and the over-speed mode, with variable amplitude and variable frequency due to the rotor pulsation; otherwise, it depended on the DFIG slip. In the synchronous mode (null slip, $s = 0$), the $I_{r(abc)}$ were direct current (DC), as shown in Figure 21.

The generated active power at the DFIG stator in all operation modes is illustrated in Figure 22. Its negative sign indicates the generator operation. Therefore, the DFIG always supplies the AC-grid by its stator.

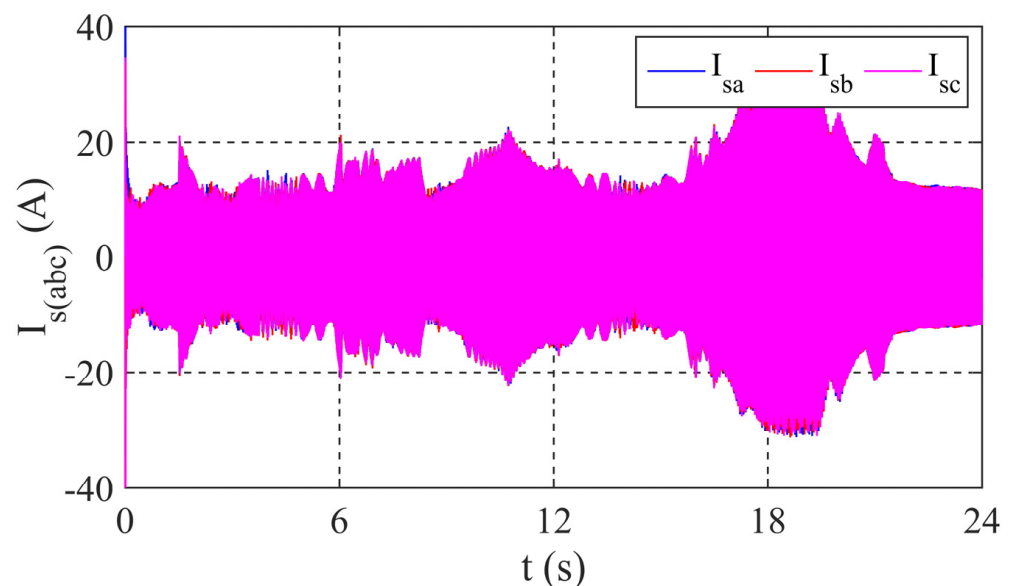


Figure 20. Evolution of the generated currents.

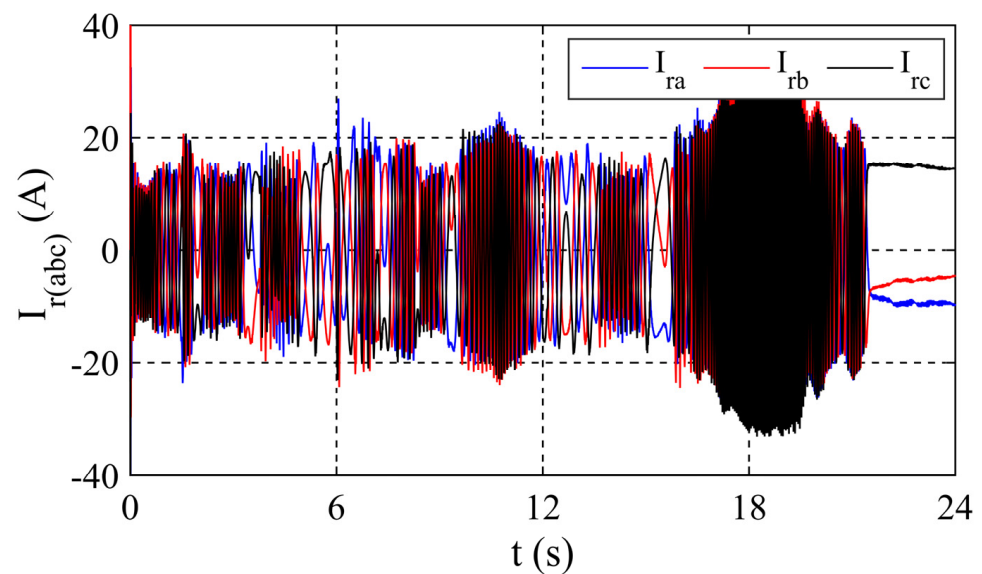


Figure 21. Evolution of the rotor currents.

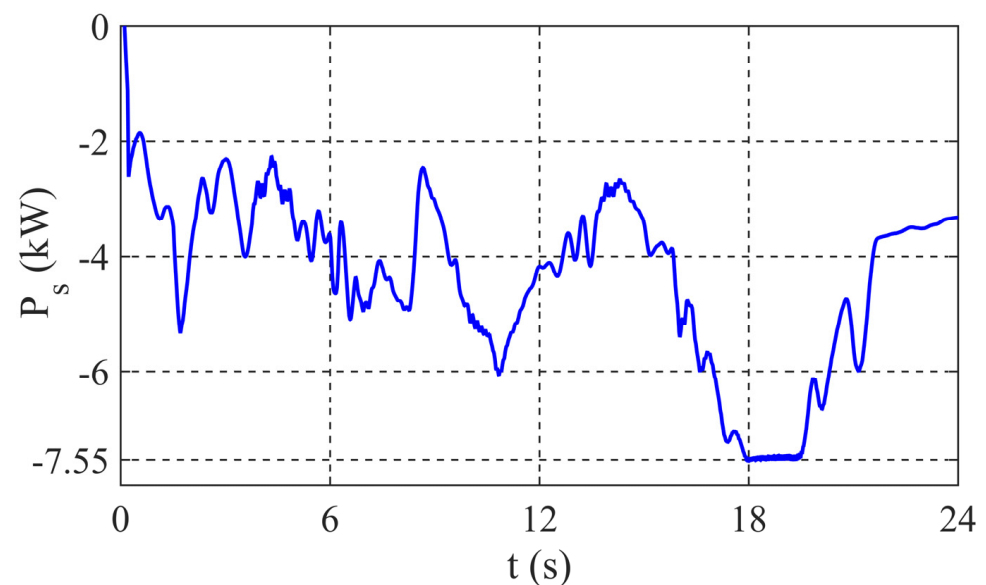


Figure 22. Generated active power waveform.

In Figure 23, the rotor active power is presented, where all DFIG modes can be clearly illustrated:

- The positive sign of the rotor active power indicates the sub-synchronous mode, where the DFIG absorbs energy from the AC-grid by its rotor.
- The synchronous mode is characterized by positive rotor active power, with a low value because it is dissipated in the rotor resistances.
- In the super-synchronous mode and the over-speed case, the rotor active power is characterized by a negative sign, where the rotor generates active power to the AC grid.

The WT-DFIG system produces energy by its stator and rotor in two modes (the super-synchronous and over-speed modes), which characterized the most important advantages of this generator.

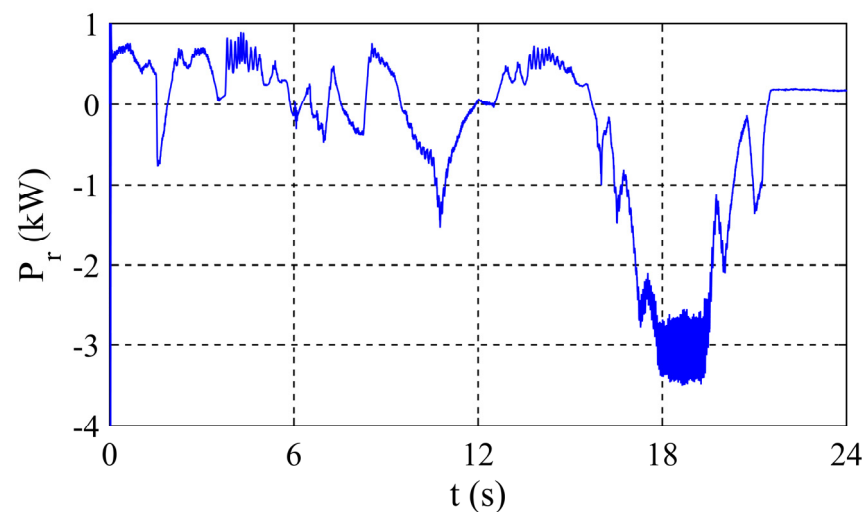


Figure 23. Rotor active power waveform.

4.2. Obtained Results Summary with Comparison

To show the improvement in the proposed control over other proposed methods in the literature [6,23,24,29–31], a comparison between the C-DTC, 12-DTC, and the proposed F12-DTC was made and is presented in Table 5 and Figures 24 and 25a–d. The rotor flux zooms are presented in Figure 24. Under the sub-synchronous mode, the φ_r was equal to: (1.200 ± 0.002) Wb, which means reductions of 77.27% and 41.17% in ripples compared to C-DTC and 12-DTC, respectively. Under the super-synchronous mode, reductions of 61.36% and 43.33% in φ_r ripples compared to C-DTC and 12-DTC, respectively, were observed. Under the over-speed mode, a reduction of 12.5% was observed compared to C-DTC, and, finally, under the synchronous mode, improvements of 76.19% and 37.5% were noticed compared to C-DTC and 12-DTC, respectively.

The electromagnetic torque ripples are presented in Figure 25. (a) Under the sub-synchronous mode, the T_{em} was equal to (-36.65 ± 0.09) N.m, which means reductions of 84.48% and 80.43% in torque ripples compared to C-DTC and 12-DTC, respectively. (b) Under the super-synchronous mode, a reductions of 85.93% and 82.69% in torque ripples were observed compared to C-DTC and 12-DTC, respectively. (c) Under the over-speed mode, a reductions of 69.92% and 39.39% were noticed compared to C-DTC and 12-DTC, respectively. Finally, (d) under the synchronous mode, an improvement of 83% in ripples compared to both C-DTC and 12-DTC was observed. Those results showed better improvement compared to both C-DTC and 12-DTC. The treatment of all operation modes under random wind speed behavior in a continuous and successive manner has not been taken into account in all references [23–31], which have treated the DTC in a general way.

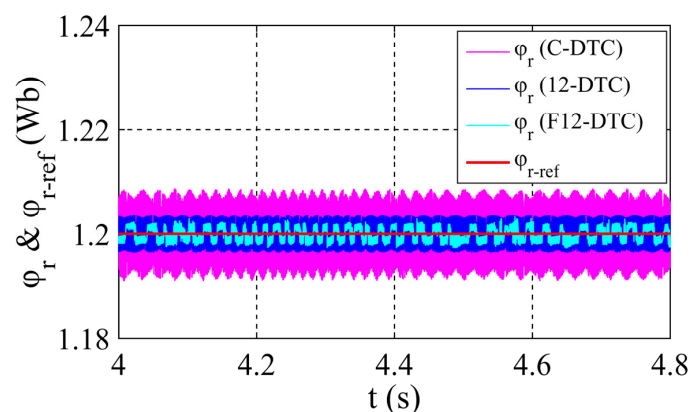


Figure 24. Rotor flux ripples of C-DTC, 12-DTC, and the proposed F12-DTC.

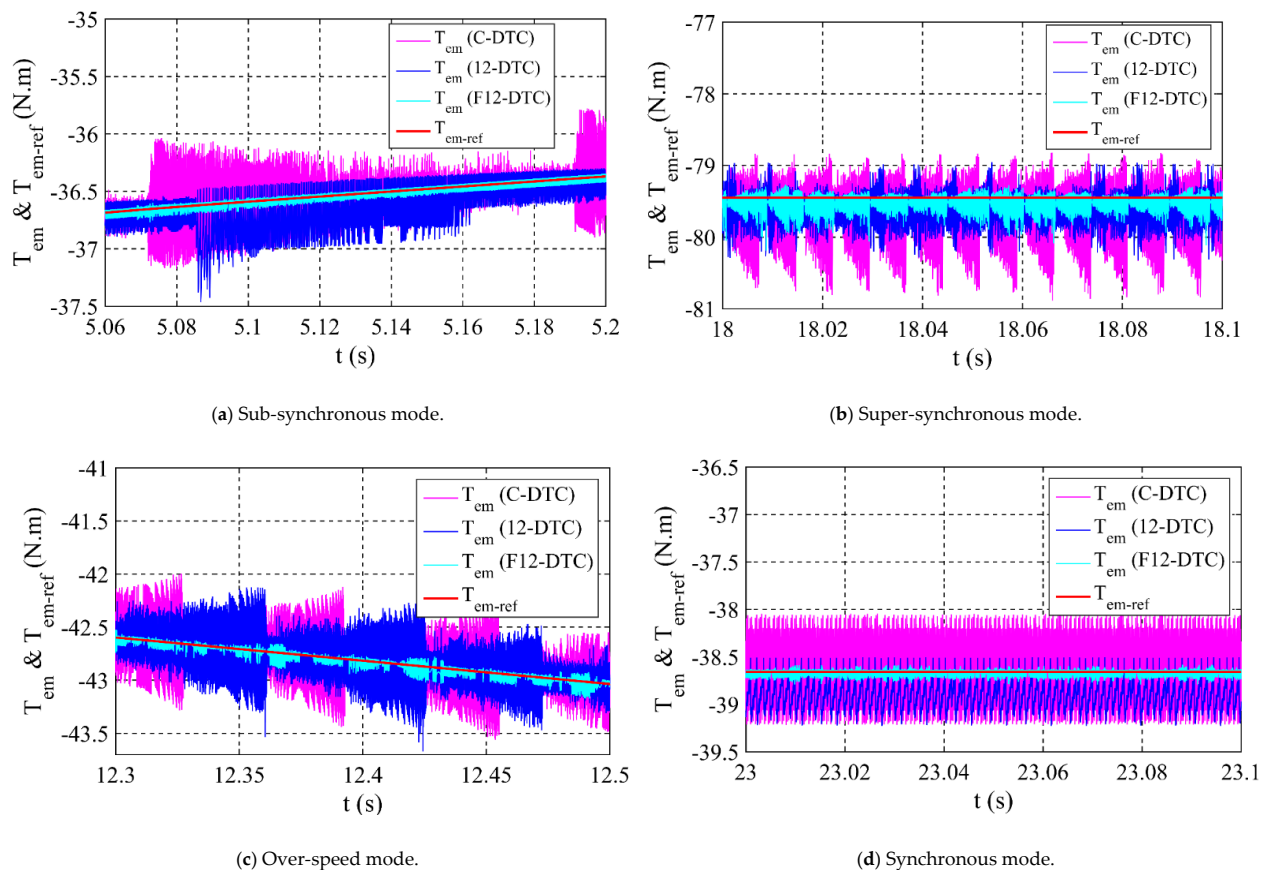


Figure 25. Electromagnetic torque ripples under the three operation modes and the over-speed mode of C-DTC, 12-DTC, and the proposed F12-DTC.

Table 5 presents the electromagnetic torque ripples and rotor flux ripples during the three DFIG operating modes and the overspeed case, as well as the rate of improvement in torque and flux-ripple reduction controlled by the proposed F12-DTC compared to both C-DTC and 12-DTC. As shown in this table, the ripples of both torque and flux are important in the studied system controlled by C-DTC and 12-DTC compared to the proposed F12-DTC. However, they were less with 12-DTC over the C-DTC. Therefore, the reduction rate of ripples was very significant in the case of the proposed F12-DTC. The average rate of improvement in torque-ripple reduction controlled by the proposed F12-DTC compared to C-DTC was 80.83%, and it was also important compared to the 12-DTC by 71.37%, where this was later less compared to C-DTC. On the other hand, the average rate of flux-ripple reduction controlled by the proposed F12-DTC compared to C-DTC was 56.83%, and it was less important compared to 12-DTC by 30.5%. These results confirmed the high performance of the proposed F12-DTC over the C-DTC and the 12-DTC.

In fact, the important ripples of both the rotor flux and the electromagnetic torque have a direct influence on the degradation of the power quality that is injected to the electrical AC grid as well as the increase in energy losses (in the converters and the generator), which will degrade the efficiency of the global system. In addition, these ripples have an influence on the turbine, the gear box, and the DFIG; they will have more mechanical vibrations, and these will increase the mechanical failures, which decreases the system life-time. Additionally, the generated currents injected to the AC grid must have a good quality. Therefore, the harmonics measurement is required in the power generation system, in order to analyze the quality instantly, as cited in [37]. Accordingly, the fast Fourier transform (FFT) analysis was made with the generated currents in order to determine the current THD. The results are presented in Figure 26, and they show a low THD (<1.8%) keeping a constant frequency of the AC grid (50 Hz).

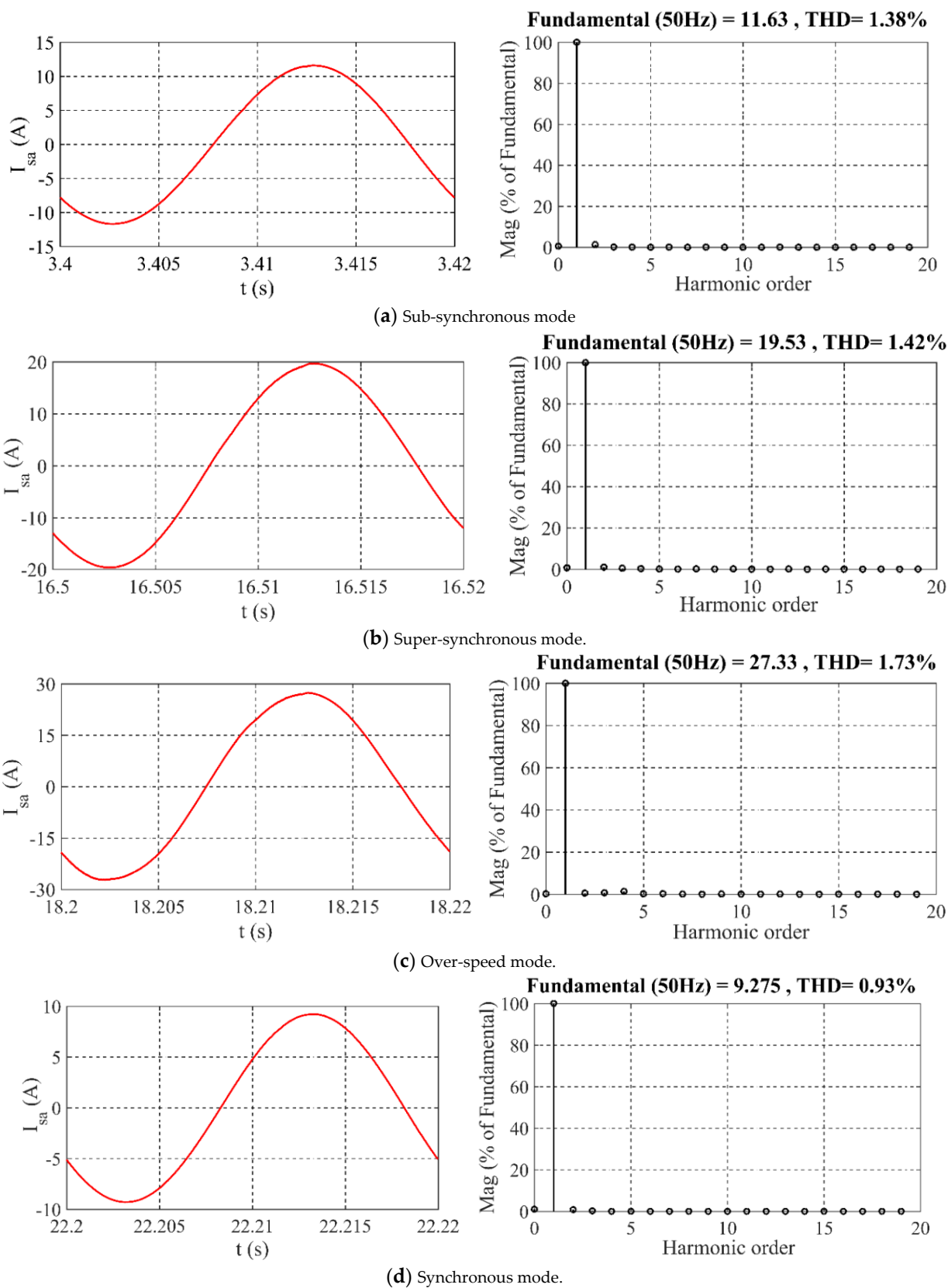


Figure 26. FFT analysis of generated current waveform of phase (a) for the three operation modes and the over-speed mode.

Table 5. Comparative analysis of rotor flux and electromagnetic torque ripples of the proposed F12-DTC and the conventional controls (C-DTC and 12-DTC).

Performances	Operation Modes				Average	
	Sub-Synchronous	Super-Synchronous	Synchronous	Over-Speed		
φ_r (Wb)	C-DTC	1.2000 ± 0.0088	1.2000 ± 0.0088	1.2000 ± 0.008	1.2000 ± 0.0084	1.2000 ± 0.0085
	12-DTC	1.2000 ± 0.0034	1.2000 ± 0.0060	1.2000 ± 0.007	1.2000 ± 0.0032	1.2000 ± 0.0049
	F12-DTC	1.2000 ± 0.0020	1.2000 ± 0.0034	1.2000 ± 0.007	1.2000 ± 0.0020	1.2000 ± 0.0036
	Ripple reduction rate of F12-DTC compared to C-DTC	77.27%	61.36%	12.5%	76.19%	56.83%
	Ripple reduction rate of F12-DTC compared to 12-DTC	41.17%	43.33%	0.00%	37.5%	30.5%
T_{em} (N.m)	C-DTC	−36.65 ± 0.58	−42.63 ± 0.64	−38.66 ± 0.54	−79.45 ± 1.33	$T_{em} \pm 0.77$
	12-DTC	−36.65 ± 0.46	−42.63 ± 0.52	−38.66 ± 0.54	−79.45 ± 0.66	$T_{em} \pm 0.54$
	F12-DTC	−36.65 ± 0.09	−42.63 ± 0.09	−38.66 ± 0.09	−79.45 ± 0.40	$T_{em} \pm 0.16$
	Ripple reduction rate of F12-DTC compared to C-DTC	84.48%	85.93%	83.00%	69.92%	80.83%
	Ripple reduction rate of F12-DTC compared to 12-DTC	80.43%	82.69%	83.00%	39.39%	71.37%

5. Conclusions

In the present study, a novel control strategy was proposed to design the desired system dynamics, to highlight the efficacy of the proposed system, and to improve the performance of the closed-loop system. The proposed controller combines the new twelve-sector methodology direct torque control (12-DTC) and a fuzzy logic controller with modified rules to solve the WT-DFIG system constraints and the drawbacks faced by the conventional methods. All DFIG operation modes were considered to reflect the true operation subject to a random wind speed. The real wind had a random behavior, which can drive DFIG under all its operating modes (sub, super, and synchronous modes); all these modes with the over-speed case were treated in this work. The high performances of the proposed F12-DTC method applied to the DFIG driven-by-WT system were established and compared with the C-DTC with 6 and 12 sectors. The simulation results showed clearly satisfactory performance with a considerable reduction in torque and flux ripples, good dynamic responses, and a low THD (<1.8%) of the generated current with a constant grid frequency of 50 Hz. In future works, we intend to focus on the implementation of the proposed F12-DTC strategy and the application of other AI techniques.

Author Contributions: Conceptualization, Y.S.; methodology, Y.S. and S.T.; software, Y.S.; validation, S.T., S.B. and S.L.B.; formal analysis, N.U.; investigation, Y.S., S.T., S.L.B. and S.B.; resources, Y.S.; data curation, S.T.; writing—original draft preparation, Y.S.; writing—review and editing, N.U., S.T. and S.L.B.; visualization, S.T.; supervision, S.B.; project administration, S.T.; funding acquisition, N.U., A.N.A. and A.A.A.A. All authors have read and agreed to the published version of the manuscript.

Funding: The authors acknowledge the funding of Taif University Researchers Supporting Project number (TURSP-2020/240), Taif University, Taif, Saudi Arabia.

Institutional Review Board Statement: Not applicable.

Informed Consent Statement: Not applicable.

Data Availability Statement: Not applicable.

Acknowledgments: The authors acknowledge the funding of TAIF University Researchers Supporting Project number (TURSP-2020/240), Taif University, Taif, Saudi Arabia.

Conflicts of Interest: The authors declare no conflict of interest.

Appendix A. The Matlab/Simulink Model Scheme of the Studied System with Explanations about the Implementation

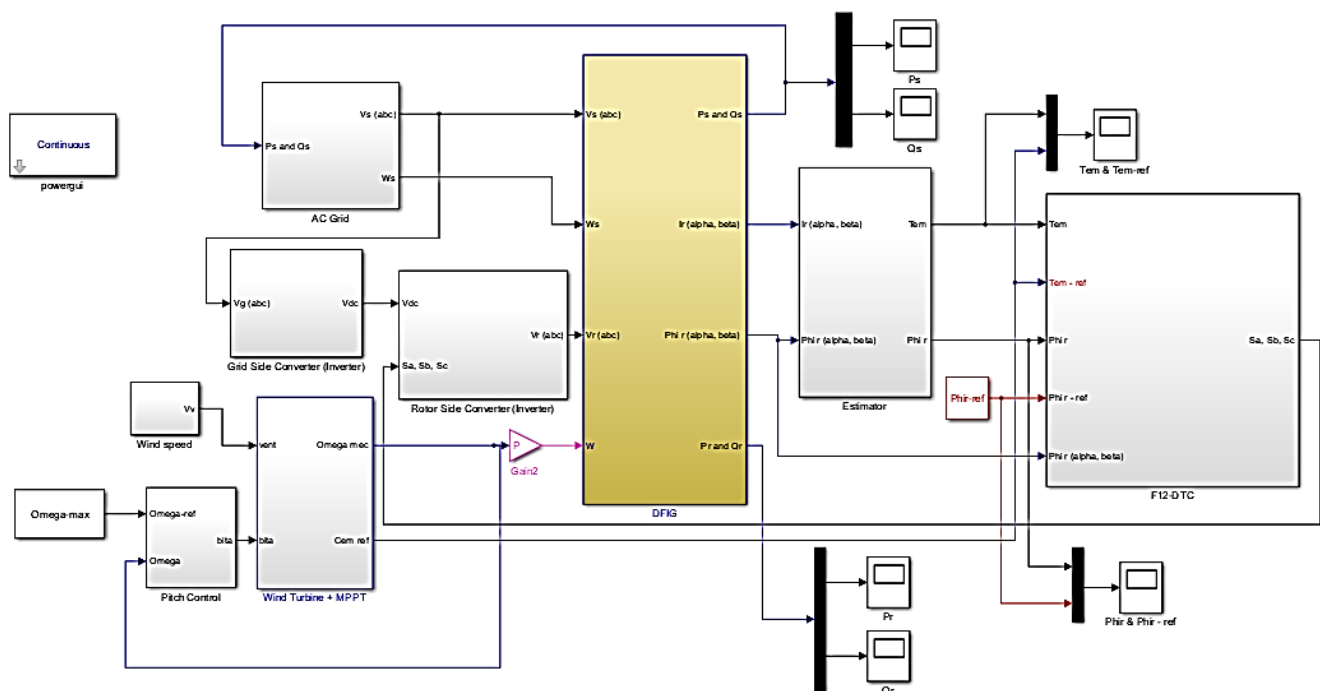


Figure A1. The simulation scheme of the global system controlled by the proposed F12-DTC.

Every sub-system was made and tested separately using the equations of the mathematical model of each system, which are given in the article: the WT, the MPPT, the pitch angle control, the DFIG, the estimator, and the proposed F12-DTC control method.

References

- Barambones, O. Robust wind speed estimation and control of variable speed wind turbines. *Asian J. Control.* **2019**, *21*, 856–867. [CrossRef]
- Yang, J.; Fang, L.; Song, D.; Su, M.; Yang, X.; Huang, L.; Joo, Y.H. Review of control strategy of large horizontal-axis wind turbines yaw system. *Wind. Energy* **2021**, *24*, 97–115. [CrossRef]
- Sahri, Y.; Tamalouzt, S.; Hamoudi, F.; Belaid Lalouni, S.; Bajaj, M.; Alharthi, M.M.; Alzaidi, M.S.; Ghoneim, S.S.M. New intelligent direct power control of DFIG-based wind conversion system by using machine learning under variations of all operating and compensation modes. *Energy Rep.* **2021**, *7*, 6394–6412. [CrossRef]
- Nobela, O.N.; Bansal, R.C.; Justo, J.J. A review of power quality compatibility of wind energy conversion systems with the South African utility grid. *Renew. Energy Focus* **2019**, *31*, 63–72. [CrossRef]
- Sahri, Y.; Tamalouzt, S.; Belaid Lalouni, S. Enhanced Direct Power Control Strategy of a DFIG-Based Wind Energy Conversion System Operating Under Random Conditions. *Period. Polytech. Electr. Eng. Comput. Sci.* **2021**, *65*, 196–206. [CrossRef]
- Tamalouzt, S.; Idjdarene, K.; Rekioua, T.; Abdessemed, R. Direct Torque Control of Wind Turbine Driven Doubly Fed Induction Generator. *Rev. Roum. Sci. Techn. Électrotechn. Énerg.* **2016**, *61*, 244–249.
- Reza, C.; Islam, M.D.; Mekhilef, S. A review of reliable and energy efficient direct torque-controlled induction motor drives. *Renew. Sustain. Energy Rev.* **2014**, *37*, 919–932. [CrossRef]
- Abdelli, R.; Rekioua, D.; Rekioua, T.; Tounzi, A. Improved direct torque control of an induction generator used in a wind conversion system connected to the grid. *ISA Trans.* **2013**, *52*, 525–538. [CrossRef] [PubMed]
- Habetler, T.G.; Profumo, F.; Pastorelli, M.; Tolbert, L.M. Direct torque control of induction machines using space vector modulation. *IEEE Trans. Ind. Appl.* **1992**, *28*, 1045–1053. [CrossRef]
- Agha Kashkooli, M.R.; Madani, S.M.; Sadeghi, R. Improved direct torque control of DFIG with reduced torque and flux ripples at constant switching frequency. In Proceedings of the 2016 7th Power Electronics, Drive Systems and Technologies Conference (PEDSTC 2016), Tehran, Iran, 16–18 February 2016; pp. 58–63. [CrossRef]
- Wong, K.C.; Ho, S.L.; Cheng, K.W.E. Direct torque control of a doubly-fed induction generator with space vector modulation. *Electr. Power Compon. Syst.* **2008**, *36*, 1337–1350. [CrossRef]
- Payam, A.F.; Hashemnia, M.N.; Faiz, J. Robust DTC control of Doubly Fed Induction machines based on input-output feedback linearization using recurrent neural networks. *J. Power Electron.* **2011**, *11*, 719–725. [CrossRef]

13. Boulouiha, H.M.; Allali, A.; Laouer, M.; Tahri, A.; Denai, M.; Draou, A. Direct torque control of multilevel SVPWM inverter in variable speed SCIG-based wind energy conversion system. *Renew. Energy* **2015**, *80*, 140–152. [[CrossRef](#)]
14. Song, D.; Chang, Q.; Zheng, S.; Yang, S.; Yang, J.; Joo, Y.H. Adaptive Model Predictive Control for Yaw System of Variable Speed Wind Turbines. *J. Mod. Power Syst. Clean Energy* **2021**, *9*, 219–224. [[CrossRef](#)]
15. Kalamian, N.; Verij Kazemi, M.; Gholomian, S.A. Direct power control of DFIG by using nonlinear model predictive controller. *Asian J. Control.* **2016**, *18*, 985–999. [[CrossRef](#)]
16. Mokhtari, M.; Davari, S.A. Predictive torque control of DFIG with torque ripple reduction. In Proceedings of the 2016 IEEE International Conference on Power and Energy (PECon), Melaka, Malaysia, 28–29 November 2016; pp. 763–768. [[CrossRef](#)]
17. Zhang, Y.; Li, Z.; Wang, T.; Hu, J.; Zhu, J. Predictive direct torque and flux control of doubly fed induction generator with switching frequency reduction for wind energy applications. In Proceedings of the 2011 International Conference on Electrical Machines and Systems, Beijing, China, 20–23 August 2011; pp. 1–6. [[CrossRef](#)]
18. Abad, G.; Rodríguez, M.A.; Poza, J. Two-level VSC based predictive direct torque control of the doubly fed induction machine with reduced torque and flux ripples at low constant switching frequency. *IEEE Trans. Power Electron.* **2008**, *23*, 1050–1061. [[CrossRef](#)]
19. Bourouina, A.; Djahbar, A.; Chaker, A.; Boudjema, Z. High order sliding mode direct torque control of a DFIG supplied by a five-level SVPWM inverter for the wind turbine. *Elektrotehniski Vestn.* **2018**, *85*, 263–270.
20. Boudjem, Z.; Taleb, R.; Djeriri, Y.; Yahdou, A. A novel direct torque control using second order continuous sliding mode of a doubly fed induction generator for a wind energy conversion system. *Turk. J. Elec. Eng. Comput. Sci.* **2017**, *25*, 965–975. [[CrossRef](#)]
21. Tamalouzt, S.; Belkhier, Y.; Sahri, Y.; Bajaj, M.; Ullah, N.; Chowdhury, M.S.; Titseesang, T.; Techato, K. Enhanced Direct Reactive Power Control-Based Multi-Level Inverter for DFIG Wind System under Variable Speeds. *Sustainability* **2021**, *13*, 9060. [[CrossRef](#)]
22. Moualdia, A.; Boudana, D.; Bouchhida, O.; Wira, P. Direct Torque control based multi-level inverter and artificial neural networks of wind energy conversion system. In Proceedings of the 2016 8th International Conference on Modelling, Identification and Control (ICMIC), Algiers, Algeria, 15–17 November 2016. [[CrossRef](#)]
23. Al-Quteimat, A.; Roccaforte, A.; Schäfer, U. Performance improvement of Direct Torque Control for Doubly Fed Induction Generator with 12 Sector Methodology. In Proceedings of the 5th International Conference on Renewable Energy Research and Application, Birmingham, UK, 20–23 November 2016. [[CrossRef](#)]
24. Taleb, M.; El Haroussi, M.; Ba-Razzouk, A. Improved Direct Torque Control of a Doubly Fed Induction Generator in a Wind Energy Conversion System. In Proceedings of the 6th International Renewable and Sustainable Energy Conference (IRSEC), Rabat, Morocco, 5–8 December 2018. [[CrossRef](#)]
25. Benboughenni, H. Five-level DTC with 12 sectors of induction motor drive using neural networks controller for low torque ripple. *Acta Electrotech. Inform.* **2018**, *18*, 61–66. [[CrossRef](#)]
26. Kim, S.J.; Park, J.; Lee, D.H. A Predictive DTC-PWM using 12 Vectors for Permanent Magnet Synchronous Motor. In Proceedings of the 2019 10th International Conference on Power Electronics and ECCE Asia (ICPE 2019-ECCE Asia), Busan, Korea, 27–30 May 2019. [[CrossRef](#)]
27. Manuprasad, P.; Mohanty, K.B. Implementation of 12 Sector Fuzzy Controller for Direct Torque Control of Induction Motor. In Proceedings of the 2019 Innovations in Power and Advanced Computing Technologies (i-PACT), Vellore, India, 22–23 March 2019. [[CrossRef](#)]
28. Djeriri, Y.; Meroufel, A.; Massoum, A. Artificial neural network based direct torque control of doubly fed induction generator. *J. Electr. Eng.* **2014**, *14*, 71–79.
29. El Ouanjli, N.; Motahhir, S.; Derouich, A.; El Ghzizal, A.; Taoussi, M.; Chebabhi, A. Improved DTC strategy of doubly fed induction motor using fuzzy logic controller. *Energy Rep.* **2019**, *5*, 271–279. [[CrossRef](#)]
30. Ayri, W.; Ourahou, M.; El Hassouni, B.; Haddi, A. Direct torque control improvement of a variable speed DFIG based on a fuzzy inference system. *Math Comput. Simul.* **2018**, *167*, 308–324. [[CrossRef](#)]
31. Ayri, W.; Haddi, A. Fuzzy 12 sectors improved direct torque control of a DFIG with stator power factor control strategy. *Int. Trans. Electr. Energy Syst.* **2019**, *29*, e12092. [[CrossRef](#)]
32. Li, S.; Timothy AHaskew Yang-Ki, H.; Shukul, M. Integrating electrical and aerodynamic characteristics for DFIG wind energy extraction and control study. *Int. J. Energy Res.* **2010**, *34*, 1052–1070. [[CrossRef](#)]
33. Sahri, Y.; Tamalouzt, S.; Belaid Lalaoui, S. Direct Torque Control of DFIG Driven by Wind Turbine System Connected to the Grid. In Proceedings of the 2018 International Conference on Wind Energy and Applications in Algeria (ICWEAA), Algiers, Algeria, 6–7 November 2018. [[CrossRef](#)]
34. Lalouni, S.; Rekioua, D.; Idjdarene, K.; Tounzi, A. Maximum Power Point Tracking Based Hybrid Hill-climb Search Method Applied to Wind Energy Conversion System. *Electr. Power Compon. Syst.* **2015**, *43*, 1028–1038. [[CrossRef](#)]
35. Shaikh Mo, S.A.; Maurya, R.; Gupta, N. Modified Switching Table-Based Direct Torque Control of Six-Phase Induction Motor Drive. *Electr. Power Compon. Syst.* **2019**, *47*, 1077–1089. [[CrossRef](#)]
36. Tamalouzt, S.; Benyahia, N.; Rekioua, T.; Rekioua, D.; Abdessemed, R. Performances analysis of WT-DFIG with PV and fuel cell hybrid power sources system associated with hydrogen storage hybrid energy system. *Int. J. Hydrogen Energy* **2016**, *41*, 21006–21021. [[CrossRef](#)]
37. Sahri, Y.; Belkhier, Y.; Tamalouzt, S.; Ullah, N.; Shaw, R.N.; Chowdhury, M.S.; Techato, K. Energy Management System for Hybrid PV/Wind/Battery/Fuel Cell in Microgrid-Based Hydrogen and Economical Hybrid Battery/Super Capacitor Energy Storage. *Energies* **2021**, *14*, 5722. [[CrossRef](#)]